V European Conference on Computational Fluid Dynamics
ECCOMAS CFD 2010
J. C. F. Pereira and A. Sequeira (Eds)
Lisbon, Portugal,14-17 June 2010

SIMULATING CAVITATING FLOWS WITH LES IN OPENFOAM

Rickard E. Bensow and Göran Bark

Department of Shipping and Marine Technology
Chalmers University of Technology, S-41296 Göteborg, Sweden
e-mail: {rickard.bensow, bark}@chalmers.se

Key words: CFD, LES, Cavitation, OpenFOAM

Abstract. *In this paper, we will review and discuss recent years progress in simulating unsteady cavitating flows in OpenFOAM at the Dept. of Shipping and Marine Technology at Chalmers, and what we believe is needed to further advance predictions and reliability. Using Large Eddy Simulation together with a mixture assumption and a finite rate mass transfer modeling, we have demonstrated in our numerical simulation the presence of several cavitation mechanisms important to capture when studying cavitation nuisance for hydrodynamic machinery, such as marine propellers and power turbines. These phenomena include the presence and action of re-entrant jets, e.g. cutting of sheet cavities thus causing shedding, but also some intrinsic details of secondary cavitation influenced by shear layers and vortex roll-up. The cases that will be referred to in the discussion include a hemispherical head, a NACA0015 hydrofoil, the Delft Twist11 hydrofoil, and the INSEAN E779A propeller.*

1 INTRODUCTION

Minimizing the nuisance of cavitation is a great challenge in the design phase of a marine propeller. For efficiency reasons, the propeller usually needs to be operated in cavitating conditions but one still needs to avoid the effects of vibrations, noise and erosion. However, cavitation is a complex phenomenon not yet neither reliably assessable nor fully understood. Experimental observations can only give a part of the answer due to the obvious limitations in the measurement techniques; one example is measuring reentrant jets and internal flow, where flow features are hidden for optical measurement techniques by the cavity itself but important to study in the development of erosive cavitation. Standard simulation tools used in design typically include potential flow solvers, lifting surface or boundary element approaches, with strict theoretical limits on cavitation modeling that only in the hands of an experienced designer may give satisfactory propeller designs. Adding to the challenge is a lack of theoretical knowledge of the physical mechanisms leading to harmful cavitation and thus how to modify a design if some form of nuisance is detected.

The access of the complete flow field through Computational Fluid Dynamics, CFD, would thus be a welcome complement to experimental data in order to develop improved design guidelines. The numerical simulation of cavitation does however include many complications, both from a modeling and a computational point of view. For example is the phase change from liquid to water difficult to model on a macroscopic level and the cavitation dynamics is governed by medium to small flow scales, both in time and space, necessitating large computational grids and small time steps. Thus, the task is not straight-forward. Moreover, in order for the CFD tools to be useful in developing the physical knowledge and help the design procedure, they need to capture the correct cavitation mechanisms and it is thus not enough to use stationary conditions and global cavity characterization, such as cavity length and shedding frequencies, in the validation process.

Here, we've used an incompressible Large Eddy Simulation technique, LES, and will show its ability to capture certain mechanisms in the formation of erosive cavitation. The LES is based on an implicit modeling approach for the subgrid term and considering the flow as a single fluid, two-phase mixture. A model transport equation for the local volume fraction of vapor is solved together with the LES equations, and a finite rate mass transfer model is used for the vaporization and condensation processes. We start by describing the modeling approach in some detail, together with its implementation and point to some validation flows computed. Following this, we briefly discuss the cavitation physics necessary to simulate, and demonstrate the capability of our LES to actually capture many of these mechanisms, using a NACA0015 foil, the Delft Twist11 foil, and the INSEAN E779A propeller in a wake flow. Finally, we summarize the results and give a short outlook.

2 COMPUTATIONAL MODELING OF CAVITATING FLOWS

The physics of cavitation adds several effects that need to be considered compared with single phase hydrodynamics. The most basic ones are the presence of the two phases and the mass transfer process between water and vapor. Moreover, we have e.g. effects due to compressibility and non-condensable gases. Considering compressibility, this is mainly present in the gas phase and important in the generation of collapse pulses and rebounds, but plays also a role in the liquid flow development, related to interaction phenomena between different cavities as well as the general unsteady pressure field development. When it comes to non-condensable gases dissolved in the liquid water, this gas content will be transferred to a gaseous state during vaporization and remain in gaseous form for some time after the condensation thus leaving a clear trace of previous cavitation in the water. This affects the strength of the water and thus the cavitation dynamics if passing into a low-pressure region once more, e.g. in rudder cavitation or in turbines.

For the simulations described in this paper, we use an incompressible implicit LES approach together with a two-phase mixture assumption to account for the cavitation. This is done by introducing the vapor volume fraction and solving an additional transport equation, incorporating finite rate mass transfer models for the vaporization and condensation processes; we here consider the mass transfer models of Kunz *et al.*[21] and Sauer.[31] The solution procedure is based on a segregated PISO algorithm, but since the mass transfer models affect the velocity-pressure coupling, the pressure equation needs some special attention to increase the numerical stability. We thus neglect the above mentioned effects of compressibility and non-condensable gases, which limits the applicability of the approach and the cavitation mechanisms we can expect to capture. However, as is shown in this paper as well as previous work,[4,6,17] the methodology still seems capable of predicting many crucial mechanisms necessary in the analysis of cavitation erosion. This extends to prediction of initial generation of potentially erosive cavitation, while the capturing of detail in the collapse process requires a compressible approach and considerably higher mesh resolution.

2.1 Large Eddy Simulation

As the terminology indicates, LES is based on computing the large, energy-containing structures that are resolved on the computational grid, whereas the smaller, more isotropic, subgrid structures are modeled. This separation of scales within the flow is accomplished by a low-pass filtering of the Navier-Stokes Equations, in practice most often performed implicitly through the cell average in the finite volume method. In contrast with RANS approaches (e.g. Wilcox[38]), which are based on solving for an ensemble average of the flow, LES naturally and consistently allows for medium- to small-scale, transient flow structures. When simulating unsteady, cavitating flows, we believe this is an important property in order to be able to capture the mechanisms governing the dynamics of the formation and shedding of the cavity. Thus, starting from the incompressible Navier-Stokes

equations, the governing flow equations consisting of the balance equations of mass and momentum,

$$\begin{aligned} \partial_t(\rho\mathbf{v}) + \nabla\cdot(\rho\mathbf{v}\otimes\mathbf{v}) &= -\nabla p + \nabla\cdot\mathbf{S}, \\ \nabla\cdot(\rho\mathbf{v}) &= 0, \end{aligned} \tag{1}$$

where $\mathbf{v}$ is the velocity, p is the pressure, $\mathbf{S} = \mathbf{2}\mu\mathbf{D}$ is the viscous stress tensor, where the rate-of-strain tensor is expressed as $\mathbf{D} = \frac{\mathbf{1}}{\mathbf{2}}\left(\nabla\mathbf{v} + \nabla\mathbf{v}^{\mathbf{T}}\right)$, and μ is the viscosity. The LES equations are theoretically derived, following e.g. Sagaut,[30] from Eq. (1) by applying low-pass filtering, using a pre-defined filter kernel function $G = G(\mathbf{x}, \Delta)$, such that,

$$\begin{aligned} \partial_t(\rho\overline{\mathbf{v}}) + \nabla\cdot(\rho\overline{\mathbf{v}}\otimes\overline{\mathbf{v}}) &= -\nabla\overline{p} + \nabla\cdot\left(\overline{\mathbf{S}} - \mathbf{B}\right), \\ \nabla\cdot(\rho\overline{\mathbf{v}}) &= 0, \end{aligned} \tag{2}$$

where overbars denote filtered quantities and commutation errors have been neglected. Equation (2) introduces one new term when compared to the unfiltered Eq. (1): the unresolved transport term $\nabla\cdot\mathbf{B}$, where,

$$\mathbf{B} = \rho\left(\overline{\mathbf{v}\otimes\mathbf{v}} - \bar{\mathbf{v}}\otimes\bar{\mathbf{v}}\right) \tag{3}$$

is the subgrid stress tensor. Following Bensow and Fureby,[5] $\mathbf{B}$ can be exactly decomposed as

$$\mathbf{B} = \rho\left(\overline{\overline{\mathbf{v}}\otimes\overline{\mathbf{v}}} - \overline{\overline{\mathbf{v}}}\otimes\overline{\overline{\mathbf{v}}} + \tilde{\mathbf{B}}\right), \tag{4}$$

where now only $\tilde{\mathbf{B}}$ needs to be modeled. The most common subgrid modeling approaches, utilizes an eddy or subgrid viscosity, ν_{SGS}, similar to the turbulent viscosity in RANS, where ν_{SGS} can be computed in a wide variety of ways, see Sagaut[30] and the references therein for an overview. In this work, we have opted for implicit modeling of $\tilde{\mathbf{B}}$, meaning that no subgrid model is applied, so called implicit LES, or ILES. This is motivated by the anticipation that $\tilde{\mathbf{B}}$ is of primarily dissipative character, which can be handled by the leading order truncation term in the numerics, a property first identified by Boris *et al.*[7] and more recently discussed in Fureby[15] and Margolin *et al.*[22]

In LES, the grid in the near wall region needs refinement in all three directions compared to the free-stream resolution in order to resolve the energetic structures. In particularly, the resolution in the spanwise direction is important, as opposed to RANS where the wall normal resolution is in focus. However, for flows of engineering interest, the computational cost for a wall resolved LES, capturing the anisotropic flow structures such as streaky structures, hairpin vortices and ejection events, is too high. Instead we apply a wall model based on the logarithmic law of the wall, implemented through an adjustment of the viscosity in the cells adjacent to the wall. Although a very simple approach, it has been successfully applied to a wide range of flows, including the ILES modeling we use in this paper.[6,13,16] Assuming that $\tau_w = \nu_{BC}{}^{u_\tau}/_y$, the subgrid wall viscosity ν_{BC} can be used to enforce the velocity to comply with the law-of-the-wall, see Fureby[14] for more details.

2.2 Multiphase Modelling

To simulate cavitating flows, the two phases, liquid and vapor, need to be represented in the problem, as well as the phase transition mechanism between the two. Here, we consider a one fluid, two-phase mixture approach, introduced through the local vapor volume fraction and having the spatial and temporal variation of the vapor fraction described by a transport equation including source terms for the mass transfer rate between the phases. Adding this transport equation to the filtered equations of continuity and momentum, Eq. 2, we get

$$\begin{aligned} \partial_t(\rho\overline{\mathbf{v}}) + \nabla\cdot(\rho\overline{\mathbf{v}}\otimes\overline{\mathbf{v}}) &= -\nabla\overline{p} + \nabla\cdot\left(\overline{\mathbf{S}} - \mathbf{B}\right), \\ \partial_t\rho + \nabla\cdot(\rho\overline{\mathbf{v}}) &= 0, \\ \partial_t\alpha + \nabla\cdot(\alpha\overline{\mathbf{v}}) &= \dot{m}/\rho_v. \end{aligned} \tag{5}$$

The density ρ and viscosity μ in Eq. 5 are assumed to vary linearly with the vapor fraction,

$$\begin{aligned} \rho &= \alpha\rho_v + (1-\alpha)\rho_l, \\ \mu &= \alpha\mu_v + (1-\alpha)\mu_l, \end{aligned} \tag{6}$$

with the bulk values, ρ_v,ρ_l,μ_v, and μ_l, kept constant. Using this expression for the density in the continuity equation it's straight forward to derive the non-homogeneous velocity divergence due to the mass transfer between the phases,

$$\nabla\cdot\overline{\mathbf{v}} = \left(\tfrac{1}{\rho_v} - \tfrac{1}{\rho_l}\right)\dot{m}, \tag{7}$$

that implies that the pressure equation in the PISO algorithm needs to be modified as well.

2.2.1 Mass Transfer Modeling of Kunz *et al.*

The model we describe here is based on the ideas of Kunz *et al.*,[21] that in turn originates from the work of Merkle *et al.*[23] The final form of the model can however be considered as based on fairly intuitive, ad hoc arguments. The mass transfer here is based on different strategies for vaporization and condensation, compared with most similar models that only rely on a single expression for both creation and destruction of vapor. The vaporization, $\dot{m}^+$, is modeled to be proportional to the amount by which the pressure is below the vapor pressure and the amount of liquid present, while the condensation, $\dot{m}^-$, is based on a third order polynomial function of the vapor volume fraction,

$$\begin{aligned} \dot{m}^+ &= A^+\rho_v\left(1-\alpha\right)\frac{\min\left[0,\bar{p}-p_v\right]}{1/2\rho_l U_\infty^2} \\ \dot{m}^- &= A^-\rho_v\left(1-\alpha\right)\alpha^2 \end{aligned} \tag{8}$$

and the specific mass transfer rate is computed as $\dot{m} = \dot{m}^+ - \dot{m}^-$. Here, $\bar{p}$ is the filtered pressure, p_v the vaporization pressure and A^+ and A^- empirical constants (of dimension $[s^{-1}]$) determining the mass transfer rate. Thus, vaporization occurs when the pressure is below the vapor pressure and there exist some liquid to vaporize, while condensation is restricted to the interface region of the cavity, independent of the pressure, with a maximum at $\alpha = 1/3$ and going to zero in the pure vapor region and the pure liquid region.

2.2.2 Mass Transfer Modeling of Sauer

The approach chosen by Sauer[31] is based on expressing the vapor fraction as a function of the number of bubbles per unit volume, n_0, and the radius of the bubbles, R_b, assumed to be the same for all bubbles,

$$\alpha = \frac{V_v}{V_l + V_v} = \frac{\frac{4}{3}\pi R_b^3 n_0}{1 + \frac{4}{3}\pi R_b^3 n_0}. \tag{9}$$

Furthermore, assuming that a change in vapor volume fraction is due not only to varying bubble sizes, but also by the change of number of bubbles, we obtain

$$\frac{D\alpha}{Dt} = (1-\alpha)\frac{4\pi R_b^2 n_0}{1 + \frac{4}{3}\pi R_b^3 n_0}\frac{DR_b}{Dt}. \tag{10}$$

Now using a simplified Rayleigh equation, where the second order derivative is neglected, to get DR_b/Dt,

$$\frac{DR_b}{Dt} = -\text{sign}(p - p_v)\sqrt{\frac{2}{3}\frac{|p - p_v|}{\rho_l}}, \tag{11}$$

we arrive at

$$\dot{m} = -\rho_v(1-\alpha)\frac{3\alpha}{R_b}\text{sign}(\bar{p} - p_v)\sqrt{\frac{2}{3}\frac{|\bar{p} - p_v|}{\rho_l}}, \tag{12}$$

where Eq. 9 have been used, and R_b is expressed as,

$$R_b = (\frac{1}{\frac{4}{3}\pi n_0}\frac{\alpha}{1-\alpha})^{1/3}. \tag{13}$$

Following Kim and Brewton,[20] we introduce an asymmetry between the condensation and vaporization terms, weighting the condensation process by a factor of two. Also here it is necessary to supply parameters to the model, the initial number of bubbles per unit volume, n_0, and the initial bubble diameter, d_{Nuc}.

2.3 Discretisation and Implementation

The computational model described above has been implemented using the OpenFOAM libraries.[1] The spatial discretization is performed using a cell centered co-located finite volume (FV) method for unstructured meshes with arbitrary cell-shapes, and a multi-step scheme is

used for the time derivatives. To complete the FV-discretization the face fluxes need to be reconstructed from grid variables at adjacent cells, requiring interpolation of the convective fluxes and difference approximations for the inner derivatives of the diffusive fluxes; see Weller *et al.*[37] and Jasak[19] for more details on the discretization and the numerics used in OpenFOAM. For the simulations presented in this paper, a second order implicit time scheme is used combined with second order linear interpolation in space, except for the convective terms discussed in the next paragraph. The time step is set small enough to ensure a maximum Courant number, Co, of less than 0.5 everywhere in the computational domain. The iterative solvers are considered converged when the residuals have been reduced by a factor of 10^{-10}.

Since the present methodology is based on implicit modeling of the modified subgrid stress tensor $\tilde{\mathbf{B}}$, a slightly diffusive scheme is needed to make the leading order truncation error act as the dissipative action of the subgrid stress tensor. This can be performed using different kind of limiters and schemes, and in the present simulations a simple form is used via a TVD limited linear interpolation scheme. Several different discretization schemes have been tested and it is shown in Bensow and Liefvendahl[6] that this approach does not cause excessive numerical diffusion and yields results that are comparable to the ones achieved with a pure second order scheme together with an explicit subgrid model.

The pressure-velocity coupling is handled via a PISO (Pressure Implicit with Splitting of Operators) procedure[18] based on a Rhie&Chow-like interpolation[28] for cell-centered data. Before entering the PISO-loop, the vapor volume fraction transport equation is solved as well as a momentum predictor step. The mass transfer terms are incorporated into the pressure Poisson equation through Eq. 7 as a split source term with the part including the pressure is treated implicitly, whereas the rest is treated explicitly, similar to what was done by Kunz *et al.*[21]

2.4 Basic Validation of the Computational Model

The LES approach and its implementation described above has been extensively validated for non-cavitating flows, and a complete discussion will not be repeated here; the references cited below include both the implicit approach we use in cavitating flows, as well as different explicit subgrid models. The published cases range from basic soundness demonstration cases, like a channel flow,[14] through canonical flows, e.g. past a circular cylinder,[11,27] to more advanced cases like the Darpa SubOFF[5,13,24] or the INSEAN E779A propeller.[6]

When it comes to quantitative validation of cavitating flows, we here report simulations of the cavitation on a hemispherical head shape at 0° angle of attack at $Re = 1.36 \cdot 10^5$, experimentally investigated by Rouse and McNown.[29] This case was introduced as soundness check for cavitating flows by Kunz *et al.*[21] and it has been repeated by several authors, e.g. Vaidyanathan *et al.*,[36] Senocak and Shyy,[32] and Ahuja *et al.*[2] Our simulations were performed as transient in a fully three-dimensional domain in order to mimic the configurations used for our more advanced cases. Both the wetted flow and the cavitating flow at $\sigma = 0.40$ have been simulated with good results for both the Kunz and the Sauer model. The grid used contained 2.2 million hexahedral cells with the parameters set to $A^+ = 2 \cdot 10^4$ and $A^- = 10^3$ in the Kunz model and in the Sauer model the initial bubble density per unit volume $n_0 = 2 \cdot 10^8$ and the initial bubble nuclei diameter $d_{nuc} = 1 \cdot 10^{-4}$ were used; and both cases the density ratio was $\rho_l/\rho_v = 1000$, which is generally considered enough. In Fig. 1, the pressure distribution is

plotted for both mass transfer models together with experimental data, as well as an isosurface of the vapor fraction together with the pressure distribution in a plane. As can be observed, the simulated results agrees well with experimental data for both the wetted and the cavitating flow, and for both the Kunz and the Sauer model. We noted some minor unsteadiness of the cavity in the simulations, as can be physically expected, and we here report average values.

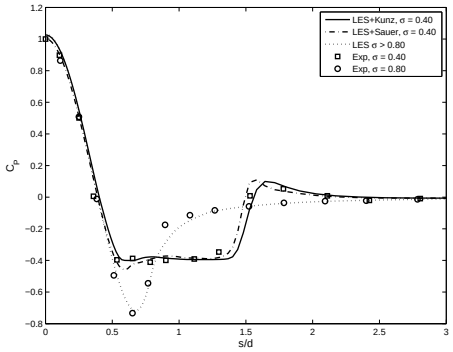

(a)

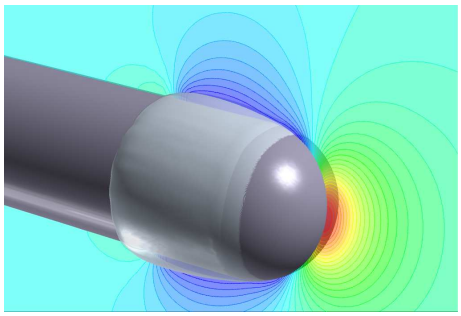

(b)

Figure 1: The pressure distribution on a hemispherical head shape in cavitating flow conditions; the cavity extent is indicated by an isosurface of the vapor fraction $\alpha = 0.5$.

3 SIMULATING TRANSIENT CAVITATION

The cavitation pattern on a foil in stationary inflow has a complex behavior in space as well as time in a wide span of scales, e.g. we find time scales typically ranging from microseconds to seconds. According to experimental, theoretical and numerical studies of 2D and 3D cavities, carried out by a number of authors during the last thirty years or more, the development of shedding of cavities is controlled by the action of different liquid jets inside the cavity. An extensive recent experimental study was reported by Foeth and Terwisga[12] and Foeth[10] on, among others, the Delft Twist11 foil which we've simulated and reports on below. Traditionally, these internal jets are collectively called re-entrant jets. Although thus unsteadiness and even randomness is characteristic for the development of cavities some features are regularl appearing, and are relating the collapse dynamics, and thus noise and erosion, with the global flow. Consequently such features are very important to predict in a numerical simulations if the aim is to say something about these phenomena.

In Bark *et al.*,[3] the large scale processes that may lead to erosive cavitation, and thus also noise and vibration, can be classified into five mechanisms:

- A traveling cavity (or bubble) which grows in a low pressure region,
- A shed cavity due to a re-entrant jet that fills a sheet cavity before pinching of the trailing part,
- The upstream moving collapse of a sheet
- A traveling cavity due to leading edge desinence, i.e. a cavity initially attached to the leading edge (of a foil or blade) when conditions for cavitation cease,

- Secondary cavitation, which is the formation of new cavitation in the disturbed flow, i.e. in a shear layer, due to any of the other mechanisms.

The concept of secondary cavitation is however not a distinct classification and mixed types may occur. Different types of rebounds can be considered as secondary cavitation, as well as what we call vortex group cavitation, where several small vortices are formed in a shear layer created by e.g. re-entrant jets. One additional mechanism, important especially for marine propellers, is the interaction between an attached sheet on the propeller blade and the tip vortex. Broad band noise is often related to unsteady properties of the tip vortex, and the modulation of the vortex due to the dynamics of the attached sheet is thus one of the causes for this particular noise problem.

We will demonstrate that all mechanisms except the single traveling bubble are present in our simulations, which is a very promising indication of the capacity of the technique. The re-entrant jet is responsible for the main shedding on the Twist11 foil as well as on the NACA0015. In the latter case, also the upstream moving collapse occurs. In both these cases, secondary cavitation, in the form of vortex group cavitation, is formed. To see the leading edge desinence, we need to turn to the INSEAN E779A propeller operating in a wake field. We will here also demonstrate how the developing sheet cavity on the blade interacts with the tip vortex, shifting its position as it leaves the blade. We remark however that although these mechanisms are clearly present in the simulations, more detailed validation regarding the balance between different mechanisms are needed before LES can confidently be used to assess cavitation nuisance. As already noted, some physics influencing the dynamics of the cavities are also missing, e.g. compressibility and non-condensable gas content, and the impact of these approximations needs to be further studied; work in progress at Chalmers.

3.1 Cavitation on the NACA0015 Foil

Here, a section of the foil with a span of 0.1 cords has been simulated, mounted at 10° angle of attack. The computational domain and the grid is displayed in Fig. 2. The spanwise extent is obviously too small to reliably capture three-dimensional effects, although comparing with experimental videos the spanwise structures developing seem quite reasonable. The foil is well resolved with a grid built of around 2.7 million hexahedral cells with a spanwise cell count of 70; y^+ values are between 1 and 2 everywhere except in the stagnation region. The cord is 200 mm and the inlet velocity is $u_\infty = 6$ m/s, leading to a Reynolds number of $Re = 1.08 \cdot 10^6$. The cavitation number, $\sigma = \frac{p-p_v}{0.5\rho_l u_\infty^2}$, in the simulation is $\sigma = 1.0$ and a physical density ratio was used with $\rho_l/\rho_v = 43,400$. The simulation displayed below was made using the model of Sauer[31] with initial bubble density per unit volume $n_0 = 2 \cdot 10^8$ and the initial bubble nuclei diameter $d_{nuc} = 1 \cdot 10^{-4}$, the same as for the hemispherical head shape. The case has also been simulated using the model of Kunz *et al.*[21] with the same global characterization of the cavitating flow, e.g. regarding cavity length and shedding frequency, but the mechanisms governing the cavity is not as distinctly predicted.

In Fig. 3, an isosurface of the vapor fraction $\alpha = 0.5$ is plotted during an upstream moving collapse. In frame 3(a), the main sheet is approximately at its maximum extent, and the trailing edge of the cavity is moving upstream, thus the cavity is shrinking, as we move through the frames and close to it's collapse in frame 3(f). What is more interesting is what's happening

in the wake flow of the cavity. In frame 3(b), a cavitating vortex has been shed from the main sheet which is then deformed in 3(c). The vortices displayed in frames 3(d)-3(f) are however clearly secondary cavitation, developing in the (non-cavitating) vortex that is formed in the shear between the external flow and the cavity wake flow.

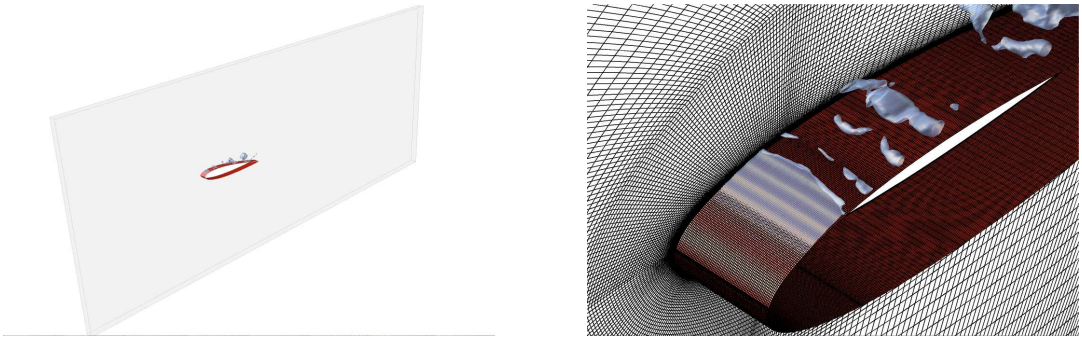

(a) (b)

Figure 2: The computational domain and a detail of the grid for the NACA0015 foil case.

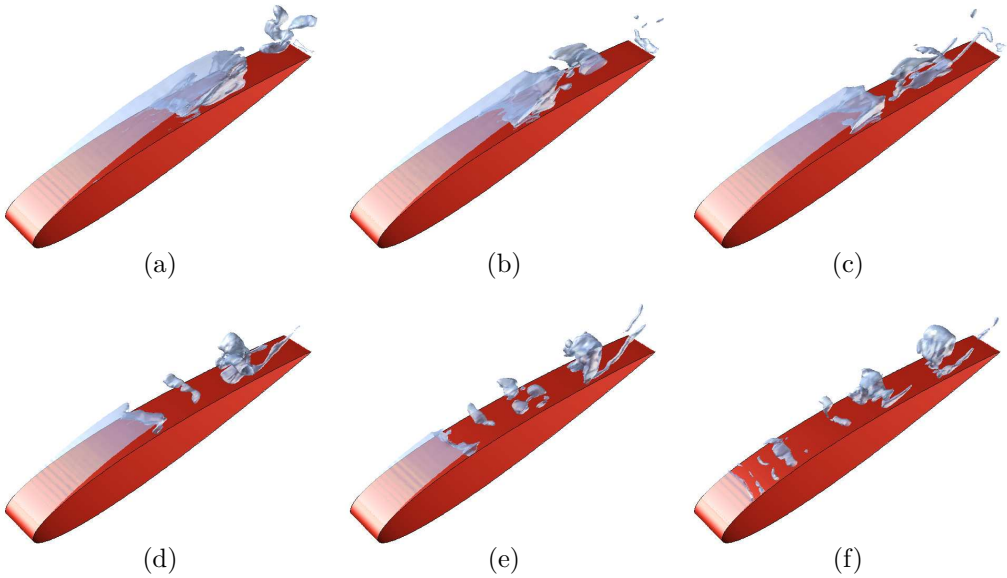

(a) (b) (c)

(d) (e) (f)

Figure 3: Upstream moving collapse on the NACA0015 foil; the cavity extent is presented using an isosurface of the vapor fraction $\alpha = 0.5$.

3.2 Cavitation on the Delft Twist11 Foil

The Delft Twist11 foil was constructed to experimentally study cavitation on a well defined geometry and location, well distanced from the walls of the cavitation tunnel, see Foeth[10] for

more information on the experiments. The cavitation that appears is similar to what occurs at the root section of a propeller blade and is thus also relevant from an engineering perspective. The geometry consists of a NACA0009 profile that has a varying angle of attack, going from 2° at the wall to 9° at the center line. The domain and grid is displayed in Fig. 4. The computational grid here consists of 2.2 M cells for the half-domain, and is thus considerably coarser than for the NACA0015 case; more typical for what we normally use in our simulations. The conditions are set to mimic the experimental set-up with an inlet velocity of $u_\infty = 6.97$ m/s, and a cavitation number of $\sigma = 1.07$; the density ratio was $\rho_l/\rho_v = 1,000$.

The simulated results are described in more detail in Huuva[17] and in Bensow *et al.*,[6] where also a summary of the experiments are included. What we show in Fig. 5 is how the re-entrant jets fill the cavity, then breaks through the sheet pinching of a part that sheds downstream, and secondary vortex cavitation is formed in the shear between the internal and external flows. In Fig. 5(a) and 5(d), the re-entrant jets has just broken up the cavity interface but a thin layer of vapor is still visible starting from the leading edge. Going further to Fig. 5(b) and 5(e), also the leading edge is here wetted, and the velocity vectors clearly display the shear layer between the re-entrant flow and the external flow; note that no vapor is present near the center plane except the larger shed structure at the trailing edge of the cavity. In Fig. 5(c) and 5(f) however, we note the two new cavitating vortices that has developed in the previously mentioned (liquid) shear layer; yet another example of secondary cavitation developing in the simulation.

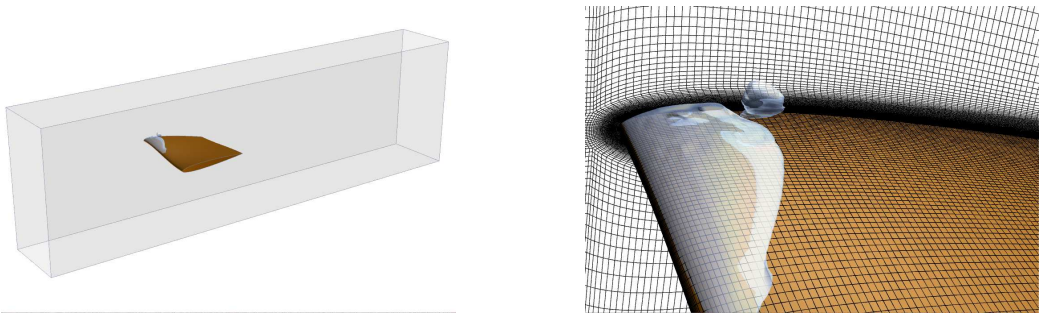

(a) (b)

Figure 4: The computational domain and a detail of the grid for the Twist11 foil case.

3.3 Cavitation on the INSEAN E779A Propeller

The final example is a propeller, originally designed in 1959 for a ferry but never built in full scale. Although being an outdated design, an extensive experimental database has been built by the research team at the Italian ship model basin, INSEAN, making it one of the best documented propellers in the open literature and thus a very interesting test case for CFD validation. Previous computational results are reported in Bensow and Liefvendahl[6] for LES in non-cavitating conditions and Bensow and Bark[4] in cavitating conditions and in Streckwall and Salvatore[35] for RANS in both non-cavitating and cavitating conditions. The propeller has been experimentally investigated in open water condition, i.e. not fitted to a hull, but with both homogeneous inflow and an artificially generated wake. Among the published data are PIV and

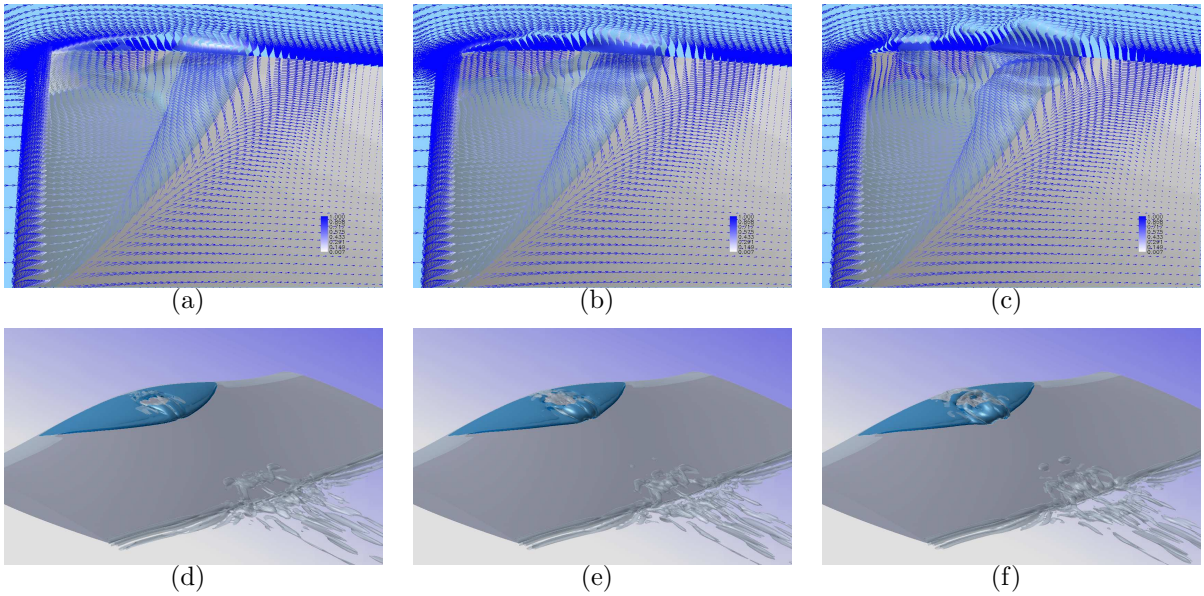

Figure 5: Formation of secondary vortex cavitation, after shedding due to re-entrant jets filling the cavity, on the Twist11 foil. In the top row, the velocity vectors close to the foil surface and on the center plane is shown, colored by the vapor fraction, and in the bottom row the cavity is indicated by a blue isosurface of $\alpha = 0.5$

LDV of the propeller wake,[8,9,33,34] cavitation pattern,[25,26] and pressure-velocity correlations.[8]

We will here only report the simulation of the propeller in cavitating conditions in an artificially generated wake; see Bensow and Bark[4] for a more complete description of our LES results on this propeller. The propeller was mounted behind a set of five plates in the cavitation tunnel and run at a cavitation number of $\sigma_n = 4.455$. Prior to the cavitation experiments, the nominal wake, i.e. without the propeller present, and the total wake was measured using LDV in a plane 0.52 R_P upstream of the propeller position, where R_P is the propeller radius. In the computations, we constructed an analytical function to approximate the nominal wake and used that as an inlet to the computation; see Fig. 6. The computational grid here is an unstructured tetrahedral grid with prism in the boundary layer with in total around 4.4 M cells. The near-wall resolution is similar to the Twist11 case and the Kunz model was used with parameters as for the hemispherical head case.

The two main features to pinpoint in this simulation is the leading edge desinence and the interaction between the sheet cavity and the tip vortex. By leading edge desinence, we mean that a cavity that is attached to the leading edge of the blade when the blade exits the wake region, where the low on-flow velocity is the cause for the cavitation, cavitation will cease on the leading edge and the cavity is turned into a travelling cavity collapsing further downstream. This can be a very erosive process and important to capture in the simulation of a cavitating propeller. This development can be seen in the innermost part of the cavity in the experimental pictures in Fig. 8(d) to 8(f). The corresponding behavior in the simulation is visible in Fig. 8(a) to 8(c). The cavity here seems however to be underpredicted, specially in Fig. 8(c), and

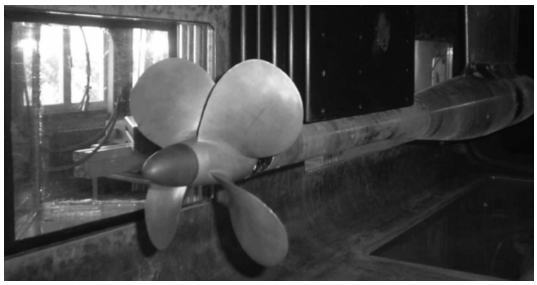

(a)

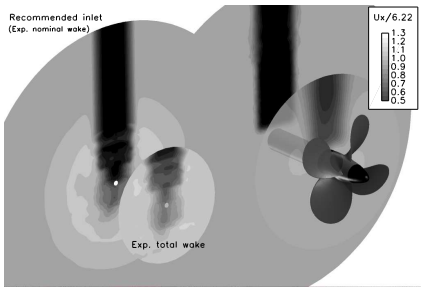

(b)

Figure 6: The experimental set-up and a comparison between the measured and computational on-flow to the propeller.

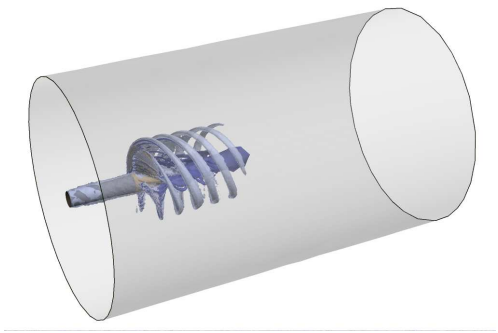

(a)

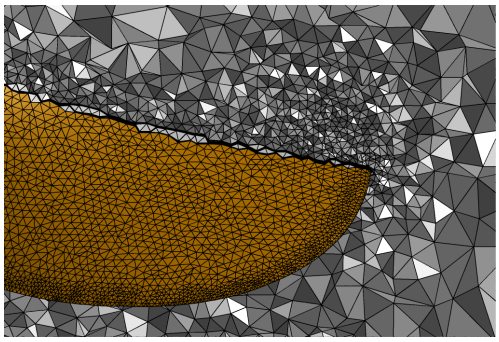

(b)

Figure 7: The computational domain and a detail of the grid for the E779A propeller.

the shed, traveling cavity cloud seem to have a higher rotation than in the computations.

In Fig 9, the influence of the sheet cavity on the tip vortex is illustrated. When the cavity is just initiated, Fig. 9(a), the tip vortex, developing due to the pressure difference between the two sides of the blade, leaves the blade exactly at the tip. However, the re-entrant jet forming around the cavity as it grows, visible through the surface streamlines in Fig. 9(b), lifts the cavity of the blade, and this affects the tip vortex which is now formed around the cavity instead of the blade tip.

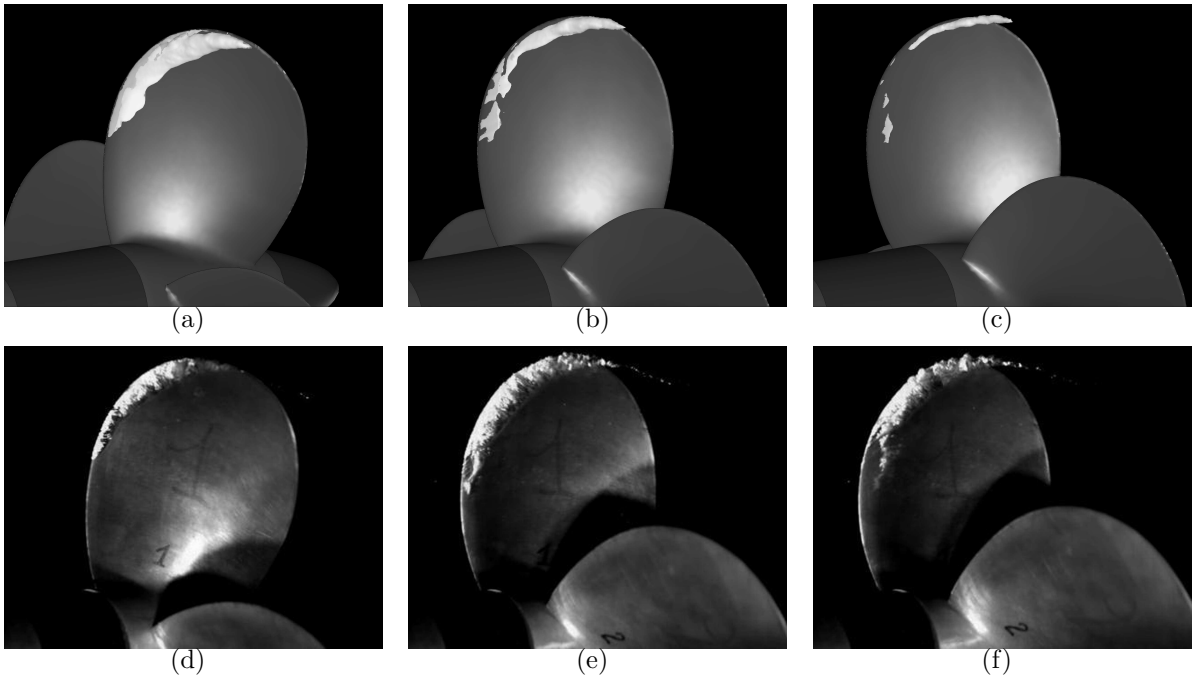

Figure 8: Development of the sheet cavity on the INSEAN E779A propeller; cavity extent in the simulated results (top row) is indicated by an isosurface of vapor fraction $\alpha = 0.5$.

4 OUTLOOK

The cases presented in this paper show that the wall-modeled, implicit LES described above have the ability to capture several important cavitation mechanisms, necessary for the prediction of cavitation nuisance such as erosion or noise. Furthermore we comment that these mechanisms are found among the large to medium-small-scale unsteady flow structures, thus raising the question if these problems can be assessed using RANS. It is however also clear that further work is needed to reach a predictive capability using LES. We argue that it's important that the main cavitation mechanisms, such as internal jets and leading edge desinence, are captured by the simulation in order to advance towards reliable predictive tools and this is clearly the case for the present modeling approach. One necessary ingredient is a high resolution in both space and time.

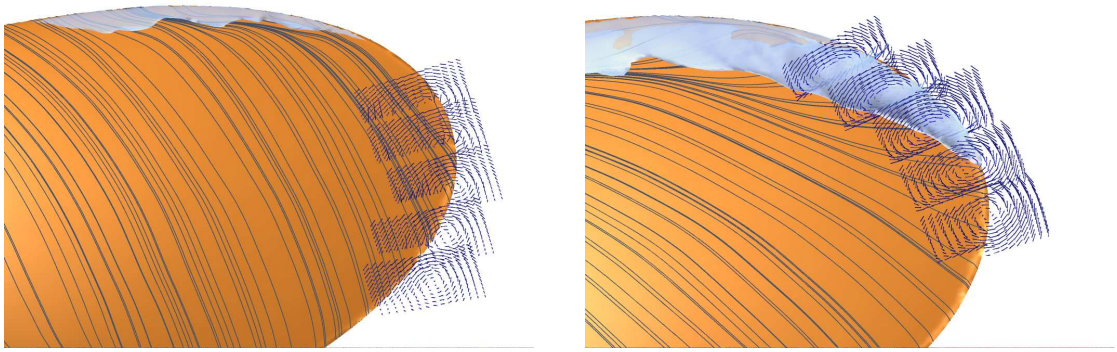

(a) (b)

Figure 9: Tip vortex development on the INSEAN E779A propeller and its interaction with the sheet cavity.

The main discrepancy when comparing the simulated results with the experimental data is the cavity extent that is not satisfactory to be useful for e.g. noise prediction. This problem seems to be fairly insensitive to parameter variations in the mass transfer model,[4] and other studies have shown that different mass transfer modeling techniques behave similarly. The two most probable causes of this discrepancy are thus believed to be related to either the resolution or the incompressible segregated solver approach.

Looking ahead, we believe that for studying the details of a cavitating flow field, LES has a great potential to become a useful and reliable tool. The short-term design cycle will for a long time be based on potential flow based methods with the capacity to predict the occurrence of cavitation and the loss of e.g. thrust, but the improved understanding of governing mechanisms that can be achieved using high-end LES will help in interpreting the results from these faster tools, as well as guiding the actual development of the design tools and principles. LES can also be part of the validation of a final design, as experiments are sometimes used today, and on the same time scale as the experiments. Such studies can preferably be done using both experimental and computational techniques, yielding complementary databases. Even though it is not yet possible to numerically predict the final collapses of cavities, the general, large-scale behavior towards the state generating approximate initial conditions for the final collapse can be studied to evaluate the risk of destructive collapses, i.e. erosion. Reliable prediction of this kind of early development, and its relation to design parameters, is clearly within reach using present cavitation modeling techniques.

To reach even further, the first natural step seems to be to include compressibility effects. This will allow one to compute a certain quantitative measure of the collapse pulse, even though a good estimate would require extremely high mesh resolutions and more sophisticated mass transfer models. More importantly, the acoustic interaction between cavities growing and shrinking and the effect of a pressure pulse on the cavitation can be captured. The inclusion of non-condensable gas content is also an important component when assessing the finer balance between the different mechanisms controlling cavitation nuisance.

5 ACKNOWLEDGEMENTS

Financial support for this work has been provided by EU FP7 project VIRTUE and by Rolls-Royce HRC through the University Technology Centre in Computational Hydrodynamics hosted at the Dept. of Shipping and Marine Technology at Chalmers. Computational resources have in part been provided by Chalmers Centre for Computational Science and Engineering, C3SE. We also like to acknowledge Tobias Huuva, presently at Berg propulsion AB, who was responsible for the simulation of the Twist11 foil when he was a PhD student at Chalmers.

REFERENCES

[1] Openfoam web site, 2008.

[2] V. Ahuja, A. Hosangadi, and S. Arunajatesan. Simulations of cavitating flows using hybrid unstructured meshes. *J. Fluids Eng.*, 123:331–40, 2001.

[3] G. Bark, M. Grekula, R. Bensow, and N. Berchiche. On some physics to consider in numerical simulation of erosive cavitation. 7th International Symposium on Cavitation, Ann-Arbor, MI, USA, 2009.

[4] R.E. Bensow and G. Bark. Implicit LES prediction of the cavitating flow on a propeller. *J. Fluids Eng.*, 2010.

[5] R.E. Bensow and C. Fureby. On the justification and extension of mixed methods in LES. *J. Turbulence*, 8, 2007.

[6] R.E. Bensow and M. Liefvendahl. Implicit and explicit subgrid modeling in LES applied to a marine propeller. Number AIAA-2008-4144, 2008.

[7] J.P. Boris, F.F. Grinstein, E.S. Oran, and R.L. Kolbe. New insights into large eddy simulation. *Fluid Dyn. Res.*, 10:199, 1992.

[8] F. Di Felice, M. Felli, G. Giordano, and M. Soave. Pressure and velocity correlation in the wake of a propeller. Propeller Shafting, Virginia Beach, Norfolk, USA, 2003.

[9] D. Di Florio, F. Di Felice, G. P. Romano, and Elefante M. Propeller wake structure at different advance coefficients by means of PIV. PSFVIP-3, Maui, Hawaii, USA, 2001.

[10] Foeth E.J. *The structure of three-dimensional sheet cavitation.* PhD thesis, Delft University of Technology, Delft, The Netherlands, 2008.

[11] A. Feymark, N. Alin, R.E. Bensow, and C. Fureby. Les of an oscillating cylinder in a steady flow. AIAA-2010-560, 2010.

[12] E.J. Foeth and T. Terwisga. The structure of unsteady cavitation. part i: Observation of an attached cavity on a three-dimensional hydrofoil. CAV2006, Wageningen, The Netherlands, 2006.

[13] C. Fureby. ILES and LES of Complex Engineering Flows. *J. Fluids Eng.*, 129:1514, 2007.

[14] C. Fureby, N. Alin, N. Wikström, S. Menon, L. Persson, and N. Svanstedt. On large eddy simulations of high Re-number wall bounded flows. *AIAA Journal*, 42:457, 2004.

[15] C. Fureby and F.F Grinstein. Large eddy simulation of high reynolds-number free and wall bounded flows. *J. Comp. Phys*, 181:68, 2002.

[16] C. Fureby and A. Karlsson. LES of the Flow Past a 6:1 Prolate Spheroid. Number AIAA-2009-1616 in 47th AIAA Aerospace Sciences Meeting, 2009.

[17] T. Huuva. *Large eddy simulation of cavitating and non-cavitating flow*. PhD thesis, Chalmers University of Technology, Göteborg, Sweden, 2008.

[18] R.I. Issa. Solution of the implicitly discretised fluid flow equations by operator-splitting. *J. Comp. Phys.*, 62(1):40–65, 1986.

[19] H. Jasak. *Error Analysis and Estimation for the Finite Volume Method with Applications to Fluid Flows*. PhD thesis, Imperial College, London, UK, 1996.

[20] Sung-Eun Kim and Susan Brewton. A multiphase approach to turbulent cavitating flows. 27th Symposium on Naval Hydrodynamics, Seoul, Korea, October 2008.

[21] R.F. Kunz, D.A. Boger, D.R. Stinebring, T.S. Chyczewski, J.W. Lindau, H.J. Gibeling, S. Venkateswaran, and T.R. Govindan. A preconditioned navier-stokes method for two-phase flows with application to cavitation prediction. *Comput. Fluids*, 29(8), 2000.

[22] L.G. Margolin and W.J. Rider. Numerical regularization: The numerical analysis of implicit subgrid models. In F.F. Grinstein, L. Margolin, and B. Rider, editors, *Implicit Large Eddy Simulation: Computing Turbulent Fluid Dynamics*. Cambridge University Press, 2007.

[23] C. L. Merkle, J. Feng, and P.E.O. Buelow. Computation modeling of the dynamics of sheet cavitation. 3rd International Symposium on Cavitation, Grenoble, France, 1998.

[24] Alin N., Bensow R.E., Fureby C., Huuva T., and Svennberg U. Current capabilities of RANS, DES and LES for submarine flow simulations. *J. Ship Research*, To appear 2010.

[25] F. Pereira, F. Salvatore, and F. Di Felice. Measurement and modeling of propeller cavitation in uniform inflow. *J. Fluids Eng.*, 126:671–679, 2004.

[26] F. Pereira, F. Salvatore, F. Di Felice, and M. Soave. Experimental investigation of a cavitating propeller in non-uniform inflow. 25th ONR Symposium on Naval Hydrodynamics, St John's, Canada, 2004.

[27] T. Persson, M. Liefvendahl, R.E. Bensow, and Fureby C. Numerical investigation of the flow over an axisymmetric hill using LES, DES and RANS. *J. Turbulence*, 7(4), 2006.

[28] C.M. Rhie and W.L. Chow. Numerical study of the turbulent flow past an airfoil with trailing edge separation. *AIAA Journal*, 21(11):1525–32, 1983.

[29] H. Rouse and J.S. McNown. Cavitation and pressure distribution, head forms at zero angle of yaw, 1948.

[30] P. Sagaut. *Large Eddy Simulation for Incompressible Flows.* Springer, New York, 3rd edition, 2006.

[31] J. Sauer. *Instationären kaviterende Strömung - Ein neues Modell, baserend auf Front Capturing (VoF) and Blasendynamik.* PhD thesis, Universität Karlsruhe, 2000.

[32] I. Senocak and W. Shyy. Interfacial dynamics-based modelling of turbulent cavitating flows, part-1: model development and steady-state computations. *Int. J. Numer. Methods Fluids*, 44(9):975–95, March 2004.

[33] A. Stella, G. Guj, and F. Di Felice. Propeller wake flowfield analysis by means of LDV phase sampling technique. *Exp. Fluids*, 28:1–10, 2000.

[34] A. Stella, G. Guj, F. Di Felice, and M. Elefante. Experimental Investigation of Propeller Wake Evolution by Means of LDV and Flow Visualizations. *J. Ship Research*, 44(3):155–169, Sept. 2000.

[35] H. Streckwall and F. Salvatore. Results of the Wageningen 2007 workshop on propeller open water calculations including cavitation. RINA CFD 2008, Southhampton, UK, 2008.

[36] R. Vaidyanathan, I. Senocak, W. Jiongyang, and W. Shyy. Sensitivity evaluation of a transportbased turbulent cavitation model. *J. Fluids Eng.*, 125:447–458, 2003.

[37] H.G. Weller, G. Tabor, H. Jasak, and C. Fureby. A tensorial approach to CFD using object oriented techniques. *Comput. Phys.*, 12:620, 1997.

[38] D.C. Wilcox. *Turbulence Modeling for CFD.* DCW Industries, Inc., La Canada, Ca, USA, 1998.